Plasma restructuring of catalysts for chemical vapor deposition of carbon nanotubes

M. Cantoro,[1,a)] S. Hofmann,[1] C. Mattevi,[2,3] S. Pisana,[1,b)] A. Parvez,[1] A. Fasoli,[1] C. Ducati,[4] V. Scardaci,[1] A. C. Ferrari,[1] and J. Robertson[1,c)]
[1]*Department of Engineering, University of Cambridge, Cambridge CB3 0FA, United Kingdom*
[2]*Dipartimento di Scienze Chimiche, University of Padova, via Marzolo 1, I-335131 Padova, Italy*
[3]*Laboratorio Nazionale TASC-CNR-INFM, ss 14, km. 163.5, I-34012 Trieste, Italy*
[4]*Department of Materials Science and Metallurgy, University of Cambridge, Cambridge CB2 3QZ, United Kingdom*

(Received 26 September 2008; accepted 28 January 2009; published online 18 March 2009)

The growth of multiwalled carbon nanotubes and carbon nanofibers by catalytic chemical vapor deposition at lower temperatures is found to be aided by a separate catalyst pretreatment step in which the catalyst thin film is restructured into a series of nanoparticles with a more active surface. The restructuring is particularly effective when carried out by an ammonia plasma. The nature of the restructuring is studied by atomic force microscopy, transmission electron microscopy, x-ray photoelectron spectroscopy, and Raman. We find that as the growth temperature decreases, there is a limiting maximum catalyst thickness, which gives any nanotube growth. Plasmas are found to restructure the catalyst by a combination of physical etching and chemical modification. Large plasma powers can lead to complete etching of thin catalyst films, and hence loss of activity. Ni is found to be the better catalyst at low temperatures because it easily reduced from any oxide form to the catalytically active metallic state. On the other hand, Fe gives the largest nanotube length and density yield at moderate temperatures because it is less easy to reduce at low temperatures and it is more easily poisoned at high temperatures. © *2009 American Institute of Physics*. [DOI: 10.1063/1.3091394]

I. INTRODUCTION

The interesting properties of multiwalled carbon nanotubes (MWCNTs) and carbon nanofibers (CNFs) have led to many studies on potential applications, and experiments have so far confirmed their usefulness for a variety of applications.[1–9] Among the various deposition techniques for CNTs and CNFs, chemical vapor deposition (CVD) has the advantage of allowing surface-bound growth and a high degree of control of growth on a wide range of substrates. CVD also allows the growth of arrays of nanotubes by patterning the thin film catalyst. The larger diameter CNFs are of interest in a similar range of applications, for example, in electrochemistry[6,7] and as field emission electron sources.[8,9]

CNFs or "filamentous carbon" can be seen as the historical precursor of CNTs,[10] and they provided some early understanding of the growth mechanism.[11–14] The low temperature limit of purely thermal growth of filamentous carbon using Fe, Co, or Ni as catalysts is about 400 °C.[15–18] This can be lowered well below 400 °C by using plasma enhanced CVD (PECVD).[19–30]

We recently reported the ability to grow single walled CNT (SWCNTs) at temperatures below those reported previously for thermal CVD growth.[31] The key to this was to separate a catalyst pretreatment or step from the growth step and if necessary to define different conditions for each step. During pretreatment, the continuous thin film catalyst restructures or dewets from the support surface, changing into a series of nanoparticles, so that its atomic surface layer becomes more activated.[24,32,33] This is most clearly seen in our *in situ* transmission electron microscopy (TEM) study, where restructuring is observed in real time.[24] Recent papers have described the operation of Fe, Co, and Ni catalysts and the role of the support oxide, as seen by photoemission.[34–36] In the present paper, we further elaborate on the role of the catalyst pretreatment step, showing that MWCNT and CNFs can be grown by thermal CVD more efficiently once the film has been restructured by plasma pretreatment. Note that the CNTs and CNFs grow in the tip-growth mode here. We take the nanotube yield (proportional to the nanotube density) as a qualitative parameter to compare the growth results from the different experiments.

II. EXPERIMENTAL DETAILS

We used polished, cleaned, *n*-type Si(100) wafers as substrates, covered with a thermally grown (40–60 nm) SiO_2 buffer/barrier layer. High purity Ni, Co, and Fe catalyst films are deposited by thermal evaporation at $<10^{-6}$ mbar base pressure. The film thickness was monitored *in situ* by quartz crystal balance and calibrated *ex situ* by atomic force microscopy (AFM, Veeco Explorer) and spectroscopic ellipsometry (J. A. Woollam Co., M-2000 V). The catalyst films are patterned by optical lithography with sub-10-μm features to facilitate characterization of the resulting nanotubes.

The MWCNTs are grown in a dc-PECVD system in a

a)Present address: IMEC vzw, Kapeldreef 75, 3001 Leuven, Belgium. Electronic mail: cantoro@imec.be.
b)Present address: Hitachi Global Storage Technologies, San Jose, CA.
c)Electronic mail: jr@eng.cam.ac.uk.

 © 2009 American Institute of Physics

Downloaded 24 Mar 2009 to 129.169.178.169. Redistribution subject to AIP license or copyright; see http://jap.aip.org/jap/copyright.jsp

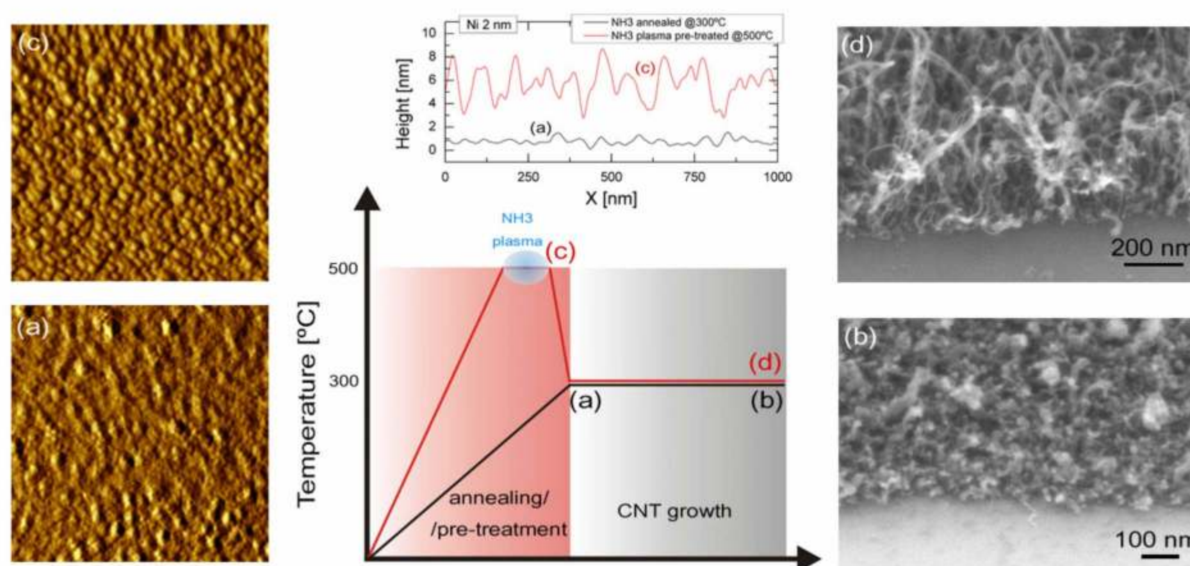

FIG. 1. (Color online) CNF growth results from [(a) and (b)] a 2 nm Ni film heated to 400 °C in NH_3 (0.6 mbar), then exposed to a 50:200 SCCM $C_2H_2:NH_3$ gas mixture (0.7 mbar) for 40 min. [(c) and (d)] A 2 nm Ni film heated up to 600 C in NH_3 (0.6 mbar), pretreated in a NH_3 plasma (600–700 V, <15 W power) for 5 min, cooled down to 400 °C while NH_3 is still flowing, and then exposed to a 50:200 SCCM $C_2H_2:NH_3$ gas mixture (0.7 mbar) for 40 min. [(a) and (c)] AFM surface scans of the 2 nm Ni film subjected to the two CNF growth routes (image scan dimensions: 1×1 μm^2). [(b) and (d)] SEM images of the corresponding as-grown CNFs. Indicated also are the AFM topography profiles along sample lines in the respective amplitude images.

stainless steel diffusion pumped vacuum chamber (base pressure $<10^{-6}$ mbar) with mass flow controlled gas feeds. The substrates are transferred in air and loaded onto a resistively heated graphite stage.

Typically, samples are first heated in only NH_3 [200 SCCM (SCCM denotes cubic centimeter per minute at STP), 0.6 mbar, flowing from a side gas inlet] to ~600 °C, then given a 5 min NH_3 plasma pretreatment in the same conditions of gas flow and pressure. The plasma is ignited by applying 600–700 V (<15 W power) between the cathode heater stage and an anode ~3 cm above it. Samples are then cooled down to the desired growth temperature while NH_3 is still flowing, and then C_2H_2 is introduced for a 50:200 SCCM $C_2H_2:NH_3$ total gas ratio at 0.6 mbar for CNF growth. Thus, in our experimental design, the pretreatment temperature is fixed, and the growth temperature is varied. Pretreated/annealed samples not exposed to hydrocarbon atmosphere do not show any growth of carbon nanostructures.

The as-evaporated and pretreated catalyst films are characterized *ex situ* by AFM (Veeco Explorer) in tapping mode at ambient conditions. As-grown CNFs are characterized by scanning electron microscopy (SEM, LEO 1530VP FEG-SEM), high-resolution transmission electron microscopy (HRTEM, Jeol JEM 4000EX, 400 kV), and Raman spectroscopy (Renishaw 1000 Raman spectrometer, 514.5 and 633 nm laser excitations). For HRTEM analysis, the CNFs are either removed from the substrates and dispersed onto Cu TEM grids or grown directly on e-beam transparent, silicon dioxide membranes (SPI Supplies).

The substrate temperature and that of the catalyst film on the processed substrate were measured by a combination of standard contact thermometry[37] and IR pyrometry (Impac IGA 8 plus).[38] The thermocouples were placed with their sensing tip onto reference Si substrates (500 μm in thickness, equivalent to samples) and the temperatures compared to those measured when the thermal contact between the thermocouple and the substrate was improved by gluing the tip to the substrate with thermal paste. Depending on the gas atmosphere and pressure in the vacuum chamber, the temperatures differ by up to 100 °C. These results were then compared to those from IR pyrometry. The temperature measured with a pyrometer represents the best estimate of the actual surface temperature, as there are no thermal contact losses. If properly calibrated against a reference temperature, the pyrometer reading should represent the upper bound of the measured surface temperature when compared with contact techniques.

The temperatures given in this paper are, by our convention, measured by a thermocouple glued to the substrate. However, literature often reports on temperature measurements performed in not fully specified conditions in the case of CVD experiments similar to ours. This can make a direct comparison of our results and some of others more difficult.

III. RESULTS AND DISCUSSION

A. Growth and AFM measurements

Figure 1 shows how a different catalyst pretreatment can drastically affect the subsequent nanofiber growth. In one case in Figs. 1(a) and 1(b), a 2 nm Ni catalyst film is heated to 400 °C in 0.6 mbar NH_3 atmosphere and then exposed to a 0.7 mbar NH_3-diluted C_2H_2 atmosphere for 40 min. In the other case in Figs. 1(c) and 1(d), a 2 nm Ni film is heated up to ~600 °C in 0.6 mbar NH_3 atmosphere and then pretreated with a NH_3 plasma for 5 min (600–700 V, <15 W power). The heater is then switched off to allow the sample to cool

Downloaded 24 Mar 2009 to 129.169.178.169. Redistribution subject to AIP license or copyright; see http://jap.aip.org/jap/copyright.jsp

down freely still in NH_3, and the heater is switched back on when the desired growth temperature (400 °C) is reached and stabilized. CNF growth then proceeds as for the former case, Figs. 1(a) and 1(b). The NH_3-annealed [Fig. 1(a)] and the NH_3 plasma pretreated 2 nm Ni films [Fig. 1(c)] are characterized by a similar topography. However, the CNF growths are distinctively different, as seen in the SEM images. CNFs grown without NH_3 plasma catalyst pretreatment in Fig. 1(b) are short and stubby. Their density is low, indicating that most of the metal did not catalyze CNF growth. For plasma pretreated catalyst, the CNF density is much larger. The CNFs are also longer and have a narrower diameter distribution, Fig. 1(d).

We previously found that different pretreatments of the same catalyst film can dramatically change the nanotube yield.[23] Annealing of subnanometer films in NH_3 or H_2, followed in the latter case by a mild restructuring in a H_2 plasma, were both found to result in SWCNT growth at low temperatures.[26] In the case of dc-PECVD, we observed a beneficial effect of a NH_3 plasma pretreatment onto 1–5 nm Ni and Co films prior to the growth stage, while the effects on Fe films were negligible.[23] Annealing in vacuum ($<10^{-6}$ mbar) was found to dramatically decrease the nanotube growth yield.

The different restructuring behaviors of the metals are due to their different interactions with the substrate (interfacial energy) and their different abilities to chemisorb gas species such as atomic hydrogen. This reflects how the catalyst surface rearranges during annealing and its subsequent reactivity, but this difference is not always obvious in topologies measured by AFM. In fact, our AFM images of Ni films after different pretreatments but at the same temperature do not have very different topologies. We note that our AFM analysis is performed *ex situ*, and so there is uncertainty due to the reoxidation of the films. We focus here on Ni as it is the least easily oxidized of the three transition metal catalysts used.

As-evaporated 1–5 nm Ni films are all characterized by a rms roughness of 0.3–0.4 nm. When annealed, a thin metal film deposited on the oxide substrate will dewet,[39] rearranging itself into nanoparticles with a diameter distribution depending on the annealing atmosphere[40] and the original film thickness,[26] increasing its roughness. Plasma pretreatment will further alter the topography of the annealed film. The extent of the reconstruction is also driven by other factors such as the plasma power, ion energy distribution, and type of radicals present. Our experiments find that a NH_3-annealed and a subsequently NH_3 plasma pretreated 2 nm Ni film have a similar topography. However, the average particle diameters are slightly smaller in the plasma case (50 nm versus 60 nm), and heights are larger (2.4 nm versus 1.4 nm). It is likely that the NH_3 plasma preferentially etches the nanoparticle edges[26] and this leads to an apparent increase in their height. If thermal annealing does not lead to a catalyst restructuring suitable for CNF growth, plasma etching can modify the catalyst surface, increasing the nucleation density for nanotube growth, especially at low temperatures. This is in accord with that found for other high-aspect-ratio nanostructures such as silicon nanowires.[41] SiH_4-plasma pretreated Au films give rise to increased nanowire growth compared to untreated films when using PECVD. This suggests that the physical effects of the plasma such as sputtering or removing nanocrystalline grains are as important as chemical effects in shaping the exposed surface.

In the literature, the pretreatment atmosphere often varies, so that a direct comparison of annealed/pretreated films is difficult. NH_3 plasmas have been deliberately used to pre-etch Ni films and increase the nanotube nucleation density.[19,22,42,43] Ren *et al.*[19] used an extended, high power plasma (50–150 W) to etch thick (>40 nm) Ni films to increase the CNT density and decrease their average diameter. However, they noted that no nanotube growth is detected when replacing NH_3 with N_2. Therefore, they concluded that there is also a beneficial effect of using NH_3 for the chemical activation of specific nucleation sites. They showed that CNT growth is sensitive to the etching gas used, although the film topology is similar. Cui *et al.*[42] used a more elaborated, two-stage NH_3 plasma etching treatment at two different temperatures. The plasma can create new nucleation sites during the film exposure to the growing atmosphere[44] while removing detrimental amorphous carbon deposited on the substrate or on the growing carbon nanostructures.[45] Choi *et al.*[46] annealed 1–10 nm Ni films at 650 °C in N_2 flow, then exposed the annealed films to a NH_3 plasma at 390 °C. Extrapolating their results, a pretreatment of a 2 nm annealed film for 10 min in a 90 W NH_3 plasma results in a distribution of island diameters of ~50 nm, quite similar to our case.

The time dependence of the plasma etching on a thin, coarsened film implies necessarily that the smallest particles are removed first. Plasma etching could then be viewed as an effective modifier of the shape of the particle distribution function, decisively narrowing it. This explains why we observe a narrower diameter distribution for nanotubes grown from pretreated films [Figs. 1(b) and 1(d)].

We previously found that an extended exposure of subnanometer catalyst films to a NH_3 plasma has the effect of etching them away completely, thus giving no SWCNT growth.[31] A milder H_2 plasma pretreatment is preferable in this case.

Figures 2–4 show the variation of the CNF growth yield with both growth temperature and catalyst thickness for Ni, Co, and Fe films, respectively. A full circle represents a high growth yield, while an empty circle represents a run without growth, in which no carbon nanostructures are found. A crossed circle represents only a few randomly sparse CNFs present. However, we stress that every circle represents a sample for which the NH_3 plasma pretreatment stage was carried out in identical conditions before CNF growth (5 min NH_3 plasma etching, <15 W, ~600 °C). Examples of CNF growth are shown in the corresponding SEM pictures (Figs. 2–4). The shaded area in Figs. 2–4 of efficient catalytic growth has a triangular shape; there is a maximum catalyst thickness for growth. This thickness decreases as growth temperature is lowered. Wei *et al.*[44] already observed this maximum thickness effect and its temperature dependence. In the case of Fe, catalyst efficiency is drastically reduced, resulting in a lower CNF yield compared to Ni below

Downloaded 24 Mar 2009 to 129.169.178.169. Redistribution subject to AIP license or copyright; see http://jap.aip.org/jap/copyright.jsp

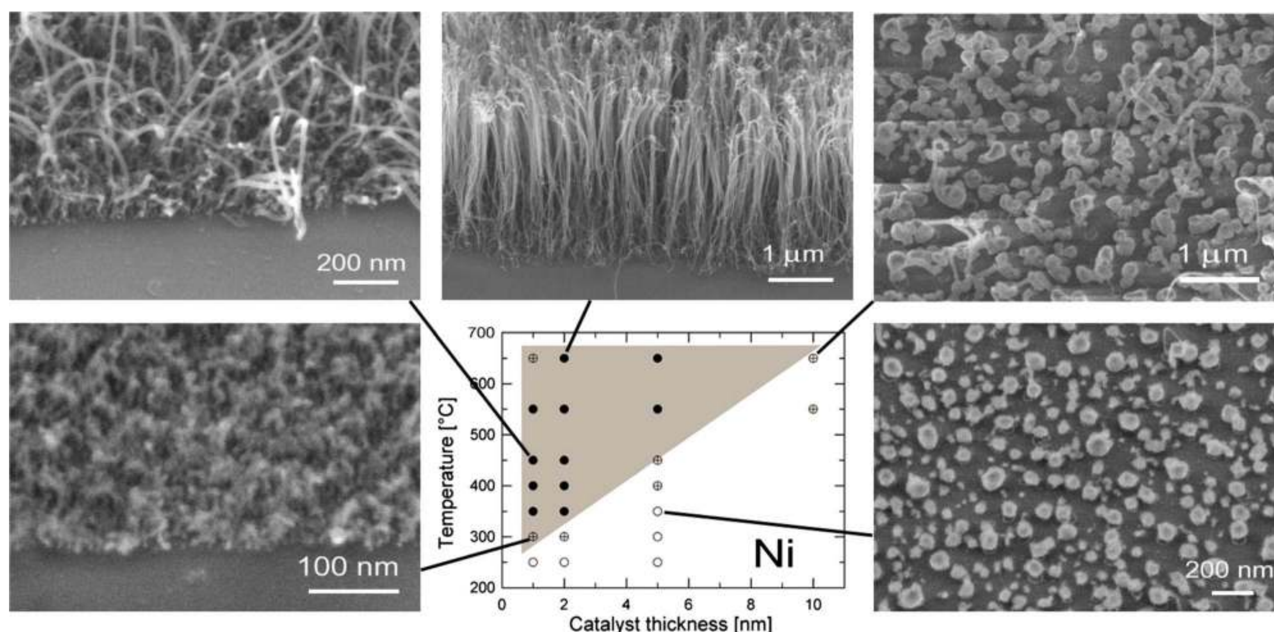

FIG. 2. (Color online) CNF growth height yield as a function of growth temperature and film thickness for Ni catalyst on Si/SiO_2. The region where the Ni catalyzes CNF growth is shaded. Sample SEM images referring to different Ni film thickness/CNF growth temperature combinations are also shown. All samples are subjected to the same pretreatment: heating up to 600 °C in NH_3 (200 SCCM, 0.6 mbar) in 15 min, followed by 5 min NH_3 plasma pretreatment (600–700 V, <15 W power).

450 °C. Co has an intermediate behavior between Ni and Fe. At high temperatures and in the 1–2 nm thickness range, the nanotube density increases dramatically for all three catalyst systems and van der Waals bundling arises.[29] All three catalyst systems have an increasing efficiency as CNF deposition temperature increases, while the thickness dependence of the efficiency peaks at 2 nm. Our plasma pretreatment conditions result in a certain catalyst particle distribution for this particular thickness value, for which our deposition conditions maximize the CNF yield. Growth saturation behavior is similar to that already observed and discussed in similar experiments.[29]

It can be difficult to estimate the length of nanotubes grown by thermal CVD when they form entangled, spaghettilike mats, whereas it is much easier if they form vertically aligned forests. Preliminary results confirm a high growth rate for Fe-catalyzed CNTs, only slightly affected by the plasma pretreatment prior to growth.[29] Ni generally gives a

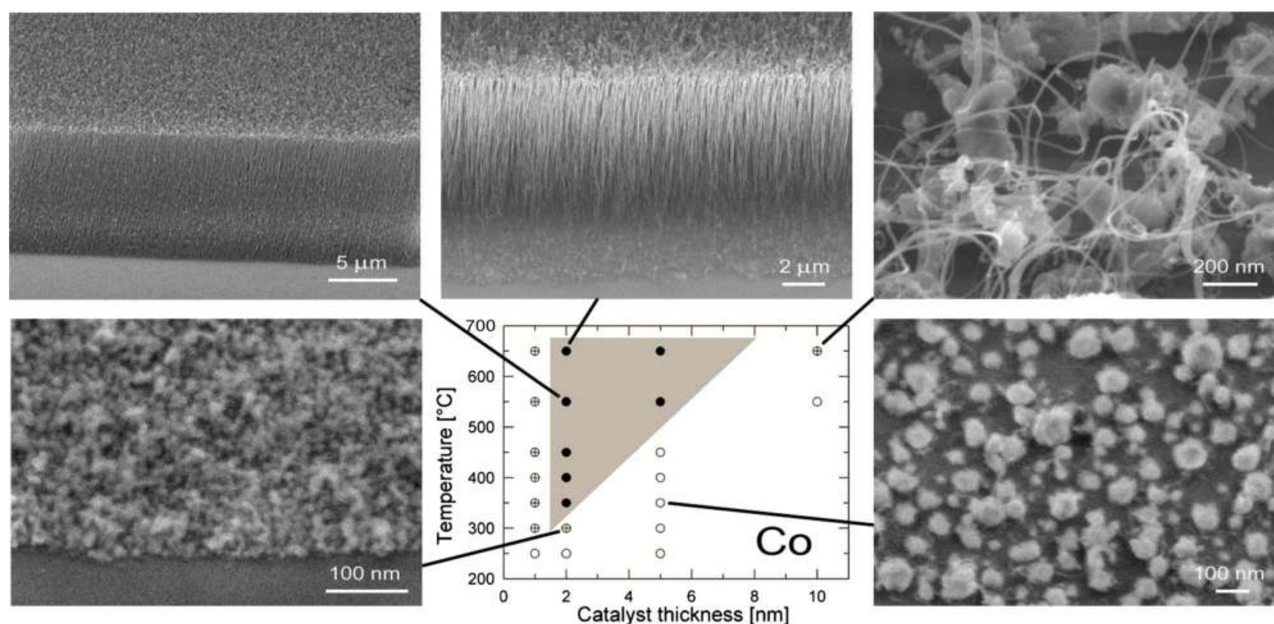

FIG. 3. (Color online) CNF growth height yield as a function of growth temperature and film thickness for Co catalyst on Si/SiO_2. The region where the Co catalyzes CNF growth is shaded. Sample SEM images referring to different Ni film thickness/CNF growth temperature combinations are also shown. All samples are subjected to the same pretreatment: heating up to 600 °C in NH_3 (200 SCCM, 0.6 mbar) in 15 min, followed by 5 min NH_3 plasma pretreatment (600–700 V, <15 W power).

Downloaded 24 Mar 2009 to 129.169.178.169. Redistribution subject to AIP license or copyright; see http://jap.aip.org/jap/copyright.jsp

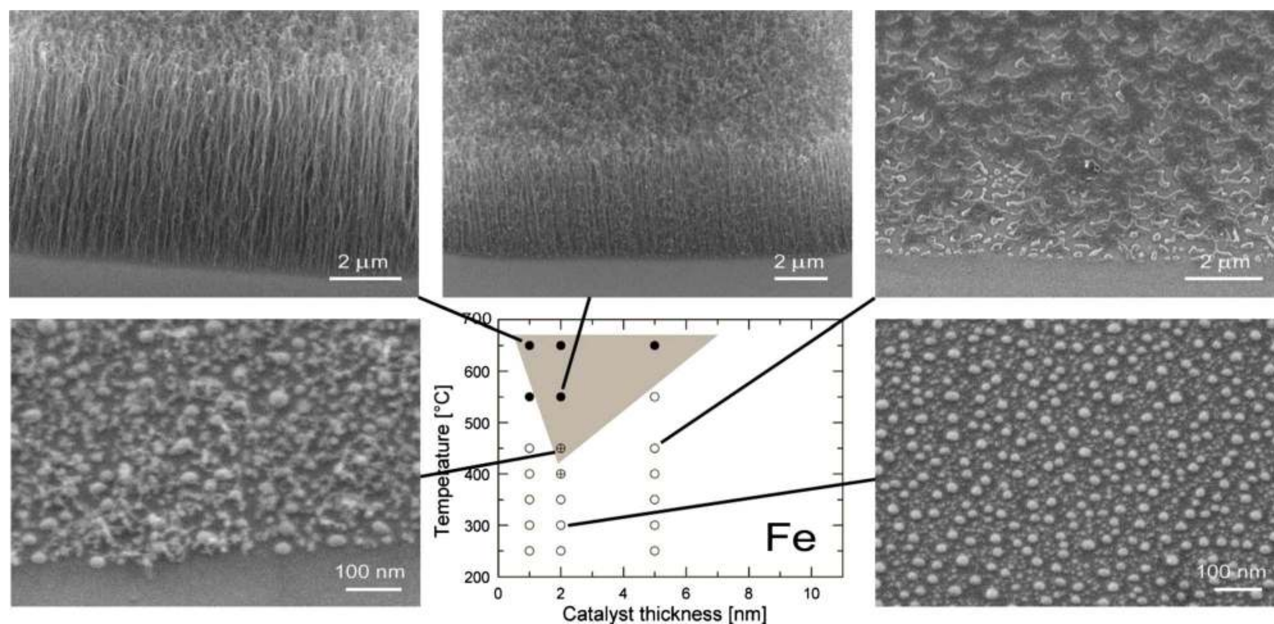

FIG. 4. (Color online) CNF growth height yield as a function of growth temperature and film thickness for Fe catalyst on Si/SiO_2. The region where the catalyst catalyzes CNF growth is shaded. Sample SEM images referring to different Ni film thickness/CNF growth temperature combinations are also shown. All samples are subjected to the same pretreatment: heating up to 600 °C in NH_3 (200 SCCM, 0.6 mbar) in 15 min, followed by 5 min NH_3 plasma pretreatment (600–700 V, <15 W power).

lower growth rate, but it catalyzes CNF growth at lower temperatures and for thicker films. We find that, for depositions carried out at ~600 °C, results strongly overlap earlier results for PECVD of nanotubes at the same deposition temperature using the same catalyst pretreatment.[23]

To assess the importance of NH_3 plasma pretreatment, we studied the dependence of the pretreatment temperature and whether it used a plasma or in purely thermal conditions, keeping the subsequent CNF growth conditions fixed (400 °C). Figure 6 shows the results of such experiments. The best growth results are obtained when the pretreatment is carried out at the highest temperature (650 °C) regardless of the use of plasma pretreatment. However, the plasma pretreatment visibly restructures the catalyst surface so that a higher CNF growth yield is achieved after the growth stage. We attribute these results to the higher extent of catalyst island restructuring occurring at higher temperatures for purely thermal effects, combined with the etching effect of the NH_3 plasma.

An NH_3 plasma is effective because it is a source of atomic hydrogen. This allows it to reduce oxides, and the volume decrease associated with this causes a transformation to metallic nanoparticles. Molecular hydrogen at low pressure is unable to reduce the oxides. This accounts for the low catalytic activity of Fe at low temperatures—it is not reduced. The second effect of the plasma is as an etchant. However, N or H do not give rise to volatile species from the metals. Thus, the main effect must be by ion bombardment from the plasma. The third effect is ion-induced mobility of surface atoms. This and the combination of ion bombardment provide etching of the metallic nanoparticles seen here,

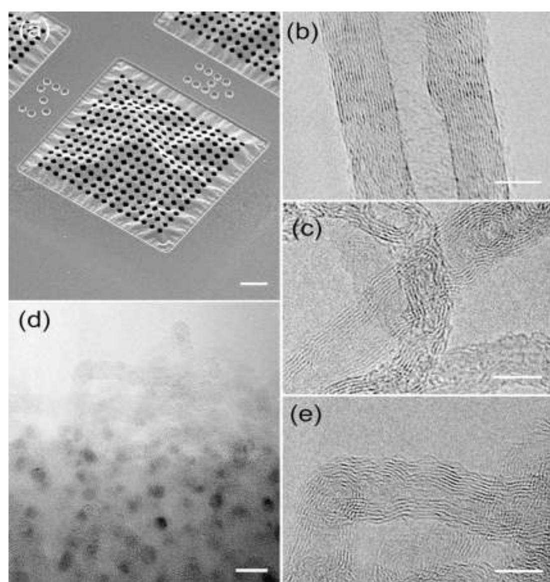

FIG. 5. HRTEM analysis of CNFs grown by thermal CVD at (b) 630 °C, [(c) and (d)] 450 °C, and (e) 350 °C from a NH_3 plasma pretreated 2 nm Ni catalyst film. Samples (c) and (e) are grown directly onto a 50 nm thick holey SiO_x membrane (a), transparent to the electron beam, while sample (b) is scratched (scale bars: (a) 10 μm, [(b), (d), and (e)] 5 nm, (c) 10 nm).

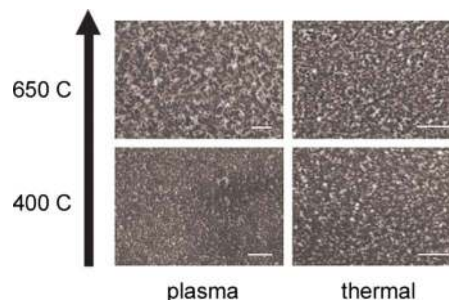

FIG. 6. (Color online) CNF growth from a 2 nm Ni film to 50:200 SCCM $C_2H_2:NH_3$ (0.7 mbar) at 400 C for 1 h showing the dependence on the film pretreatment vs plasma and thermal pretreatment and vs pretreatment temperature.

Downloaded 24 Mar 2009 to 129.169.178.169. Redistribution subject to AIP license or copyright; see http://jap.aip.org/jap/copyright.jsp

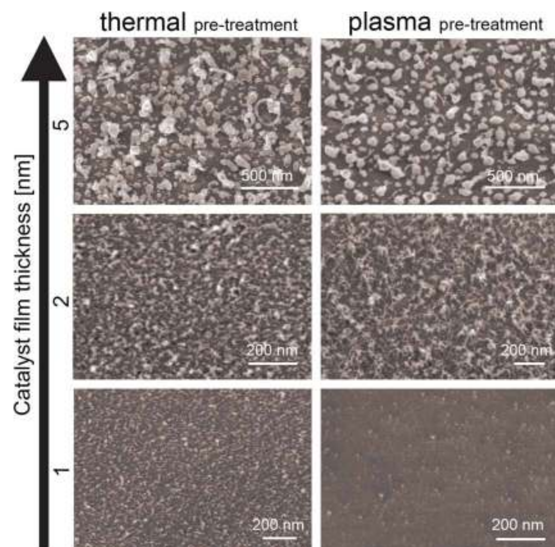

FIG. 7. (Color online) CNF growth results after exposing Ni films to 50:200 SCCM $C_2H_2:NH_3$ (0.7 mbar) at 400 °C for 1 h showing the dependence on the film pretreatment and nominal thickness. 0.3–5 nm Ni films in (a)–(c) are pretreated by heating up in NH_3 (200 SCCM, 0.6 mbar) to 650 °C in 15 min and applying a NH_3 plasma (600–700 V, <15 W) for 5 min. Films in (d)–(f) are pretreated by heating up in NH_3 (200 SCCM, 0.6 mbar) at 650 and 400 °C, respectively, in 15 min, followed by a 5 min dwell time at the same temperature and gas atmosphere.

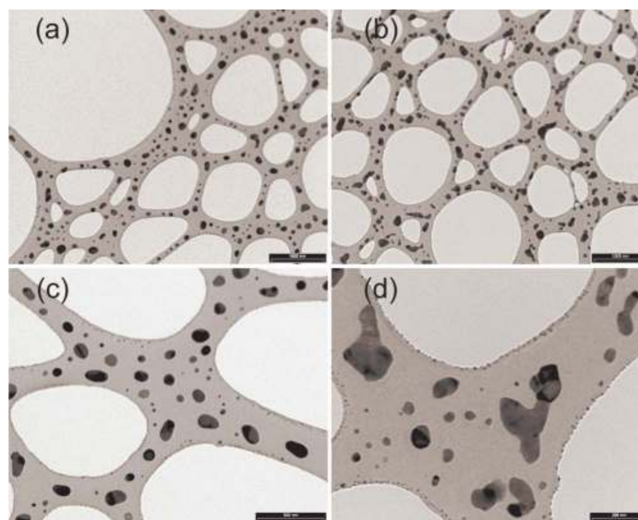

FIG. 8. (Color online) TEM images of 2 nm Ni films evaporated onto SiO_x, e-beam transparent grids, then subjected to different pretreatments. Grids in (a) and (c) are pretreated in NH_3 (200 SCCM, 0.6 mbar) at 650 °C for 15 min, followed by a 5 min dwell time at the same temperature and gas atmosphere. Grids in (b) and (d) are heated up in NH_3 (200 SCCM, 0.6 mbar) to 650 °C in 15 min and applying a NH_3 plasma (600–700 V, <15 W) for 5 min.

and particularly their sidewalls, leading to increased roughness. However, too much plasma pretreatment can remove the catalyst altogether.

Figure 7 shows the variation of the CNF growth yield with the catalyst thickness and the presence of plasma pretreatment. We notice how the NH_3 plasma pretreatment can remove the thinnest catalyst layers, thus inhibiting CNF growth. In both cases and as noted in Figs. 2–4, the highest CNF yield peaks at ~2 nm Ni film thickness. Analysis of Fig. 7 shows the extent of the chemical sputtering effect of the NH_3 plasma.

B. TEM-HRTEM analysis

HRTEM was used to study the extent of catalyst reconstruction under the thermal and plasma pretreatments and to explain the variation of CNF growth yield. Figure 8 shows low-resolution TEM images of 2 nm Ni films evaporated onto Cu TEM grids with lacey carbon onto which 20 nm SiO_x was sputtered prior to the catalyst deposition. The grid in Figs. 8(a) and 8(c) was pretreated by heating up to 650 °C in 0.6 mbar NH_3 in 15 min, then kept at the same temperature for 5 min. The grid in Figs. 8(b) and 8(d) was pretreated by heating to 650 °C in 0.6 mbar NH_3 for 15 min, then applying a dc discharge for 5 min plasma pretreatment (600–700 V, <15 W).

There is striking difference between the Ni cluster morphologies after each pretreatment. Thermally pretreated samples show Ni clusters with a smoother contour and a round/ellipsoidal shape, Figs. 8(a) and 8(c). In contrast, in Figs. 8(b) and 8(d) plasma pretreated Ni clusters have a more irregular, complex shape. The two-dimensional (2D) character of the low-resolution TEM image in Fig. 8 gives no information on the height of the clusters. We can assume that the 200–300 nm Ni clusters are polycrystalline. The complex shape can result in more nucleation sites for nanofiber growth. As the nanofibers were grown in the tip-growth regime, the single irregularly shaped Ni clusters can potentially nucleate more than one single CNF.[20]

Figure 9 shows low-resolution TEM images of the grids of Fig. 8 after exposure to the growth atmosphere (50:200 SCCM $C_2H_2:NH_3$, 0.7 mbar) at 450 °C for 5 min. The short growth time is needed to see the very early stages of growth. Figures 9(a) and 9(b) show the thermally pretreated grid and Figs. 9(c) and 9(d) the plasma pretreated grid. All the images show a carbon shell forming around the Ni clusters, assess-

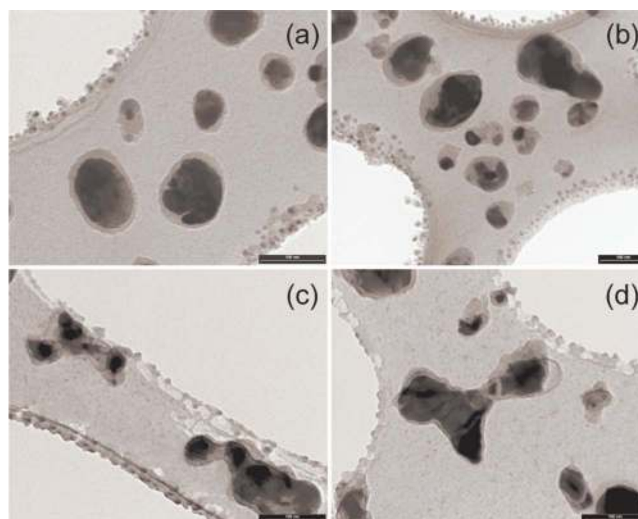

FIG. 9. (Color online) TEM images of 2 nm Ni films evaporated onto SiO_x e-beam transparent grids, exposed to 50: 200 SCCM $C_2H_2:NH_3$ (0.7 mbar) at 450 °C for 5 min subjected to different pretreatments. (a) and (b) are pretreated in 200 SCCM 0.6 mbar NH_3 at 650 °C for 15 min, with 5 min dwell time at the same temperature and gas atmosphere. Grids in (c) and (d) are in NH_3 (200 SCCM, 0.6 mbar) at 650 °C for 15 min and applying a NH_3 plasma (600–700 V, <15 W) for 5 min.

Downloaded 24 Mar 2009 to 129.169.178.169. Redistribution subject to AIP license or copyright; see http://jap.aip.org/jap/copyright.jsp

ing the onset of CNF nucleation. However, Figs. 9(c) and 9(d) show that complex shape clusters can offer more preferential sites for a CNF to grow. This will eventually lead to fragmentation of the cluster, where each fragment will be included in the tip of a growing CNF.

The HRTEM images in Fig. 5 show that the crystalline quality of CNFs grown from a 2 nm Ni film declines at lower growth temperatures, not surprisingly. We observe a transition from 10–20 walls, 10–15 nm diameter nanofibers at 630 °C [Fig. 5(b)] to 5–10 walls over 5 nm diameter CNFs grown at 350 °C [Fig. 5(e)]. CNFs grown at low temperatures are less straight and parallel and have more defective walls and a more pronounced bamboolike character. This trend is generally observed in the literature on the subject. For PECVD, low growth temperatures generally lead to poor graphitization.[23] In fact, although PECVD allows lower growth temperatures than thermal CVD, the plasma bombardment can have detrimental effects on their crystallinity. Reactive NH_x species and more generally H_2-rich plasma can etch not only the catalyst particle but also the as-grown small diameter nanotube shells,[47] even at room temperature. At high temperatures, we found that the use of plasma assistance not only affects the nanotube crystalline quality but also reduces the growth rate with respect to thermally grown nanotubes.[48] PECVD therefore requires careful optimization of plasma power and pressure to minimize disordering effects.

HRTEM images of scratched samples shows the presence of catalyst particles at the nanotube tips. This implies a tip-growth mechanism, as expected for our growth conditions.[20,22] Occasionally and especially for the highest deposition temperatures, Ni metal inclusions are found along the CNFs. For CNFs grown directly on holey SiO_x membranes [Figs. 5(c)–5(e)], the HRTEM images frequently show no catalyst at the tips. We believe that this is due to a different substrate-catalyst interaction. The membranes could have been subjected to a particular processing route. HRTEM images do not show significant differences in crystalline structure with respect to CNFs grown directly onto Si/SiO_2 substrates. Workers occasionally report a base-growth mechanism for Fe- and Co-catalyzed CNTs grown by thermal CVD (Refs. 49 and 50) or PECVD (Ref. 51) and even a transition between the two growth modes as conditions change.[52]

Many groups have noted a strong correlation between the nominal thickness of the initial catalyst layer and the resulting nanotube diameter[20,22] and density.[44] This is expected from the standard growth model, as the catalyst nanoparticle diameter dictates the outer diameter of the growing nanotube,[13] as confirmed by direct observation.[24,32,53] However, *in situ* observation also shows substantial reshaping of the catalyst during the actual process of growth and notes the importance of step edges as possible growth sites.[32,53–55]

C. X-ray photoelectron spectroscopy analysis

X-ray photoelectron spectroscopy (XPS) measurements were performed at the BESSY synchrotron in Berlin to investigate the surface chemical composition of Ni films with

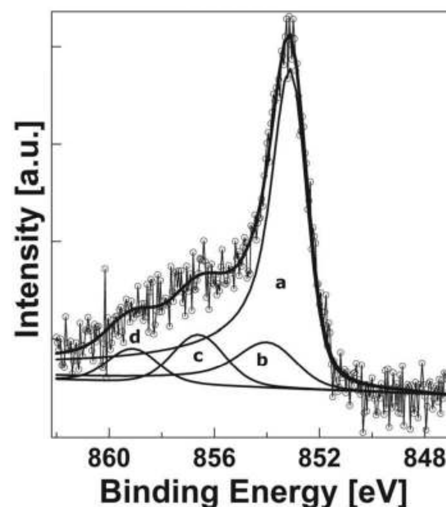

FIG. 10. Ni $2p_{3/2}$ photoemission spectrum (photon energy=1010 eV) acquired on a NH_3 plasma pretreated Ni film (2 nm) at room temperature, UHV conditions. The spectrum is normalized to the photon flux.

NH_3 plasma and nonplasma pretreatments before and after nanofiber growth using the same sample conditions. Survey scans were collected in all cases, and higher resolution spectra were recorded for detailed core level analysis (N, Ni).

When comparing spectra for plasma and nonplasma pretreated films, the first striking difference is the higher N 1*s* peak intensity for plasma treated films. A decrease in the metal core level intensity due to island formation was observed. This behavior occurred for both plasma pretreated and nonpretreated films.

Figure 10 shows the Ni $2p_{3/2}$ peak measured on a 2 nm, NH_3 plasma pretreated Ni film. The fitting procedure results in four peaks centered at 853, 853.7, 856.6, and 859 eV. Peak indexing is performed according to existing literature. Ni $2p_{3/2}$ binding energies of metallic Ni and $NiSi_x$ are 852.3 and 853.4 eV, respectively. Peaks at 853 and 853.7 eV can be assigned to Ni_xN and to a NiSiN ternary compound, respectively. We can assume that the observed Ni $2p_{3/2}$ binding energies are larger than literature values for metallic Ni and $NiSi_x$ because of the presence of N. Its electronegativity shifts the peaks to higher binding energies. There may be a small contribution of metallic Ni (853 eV) to the measured line shape in Fig. 10. Metallic Ni lies underneath a Ni_xN shell after exposure to the NH_3 plasma. The NiSiN contribution originates from the plasma nitridation of the Ni nanoparticles, alloying with the underlying SiO_2. Ni has been reported to diffuse into SiN_x even at room temperature and formation of a Ni–Si–N ternary solid solution. We stress that XPS is a surface sensitive technique and cannot resolve depths larger than 1.2 nm in our case.

The peak at 856.6 eV is due to nickel oxide. This peak is small compared to the nitride peaks and it is related to the re-exposure of the plasma treated sample to air before XPS characterization. The peak at 859 eV is the Ni_xN peak satellite.

Figure 11 shows the N 1*s* peak measured on a 2 nm, NH_3 plasma treated Ni film. The fitting procedure leads to three peaks centered at 397.9, 399.1, and 400.7 eV. We at-

Downloaded 24 Mar 2009 to 129.169.178.169. Redistribution subject to AIP license or copyright; see http://jap.aip.org/jap/copyright.jsp

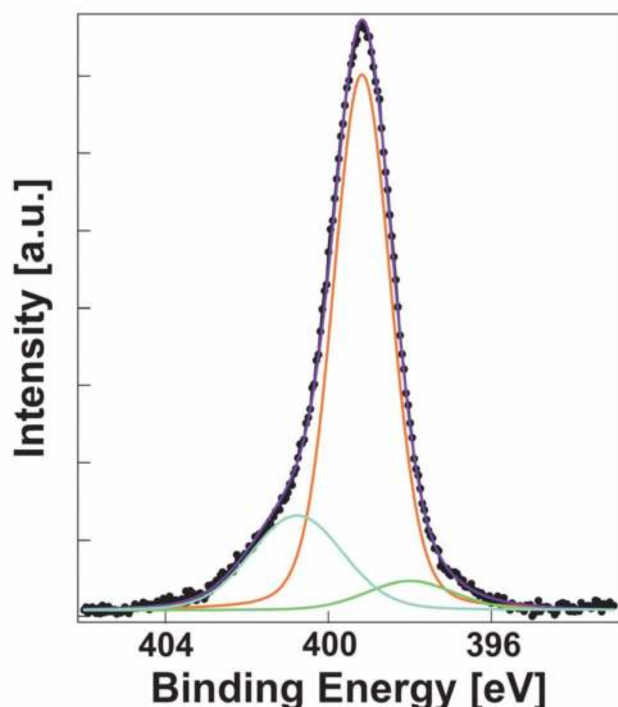

FIG. 11. (Color online) N 1*s* photoemission spectrum (photon energy =550 eV) acquired on a NH_3 plasma pretreated Ni film (2 nm) at room temperature, UHV conditions. The spectrum is normalized to the photon flux.

tribute the strongest peak at 399.1 eV to silicon oxynitride (SiO_xN_y). Nitridation of SiO_2 can occur to several nanometers for NH_3 plasma conditions similar to ours. The 400.7 eV peak is also attributed to SiO_xN_y but with higher oxygen content than the 399.1 eV peak. This is a consequence of the higher electronegativity of O than Si or N, shifting the N 1*s* peak at higher binding energies. The larger O stoichiometry could be due to more adsorbed O after re-exposure of the plasma pretreated samples to air. The 397.9 eV peak is due to Ni–N bonds in Ni_xN.

D. Raman spectroscopy

The samples were also characterized by Raman. Care was taken in order to avoid radiation damage to the samples, keeping the laser power below 10^{-9} W/m^2 (spot size ~ 1 μm^2). Our nanotubes are quite defective (Fig. 5) and their signatures could be diluted by the presence of amorphous carbon, useful structural information can be extracted by using the general framework for the interpretation of spectra of amorphous and nanocrystalline carbon.[56,57]

The spectra of CNFs grown from 2 nm Ni, Co, and Fe films are shown in Figs. 12(a)–12(d). The Raman spectra of all carbons show several common features in the 800–2000 cm^{-1} region, the so-called *G* and *D* peaks, lying at $\sim$1560 and 1360 cm^{-1} for visible excitation. The *G* peak is due to the bond stretching of all pairs of sp^2 atoms in both rings and chains, while the *D* peak is the breathing modes of sp^2 bonded rings.[56–58] Its overtone, the 2D peak, lies at $\sim$2700 cm^{-1}.

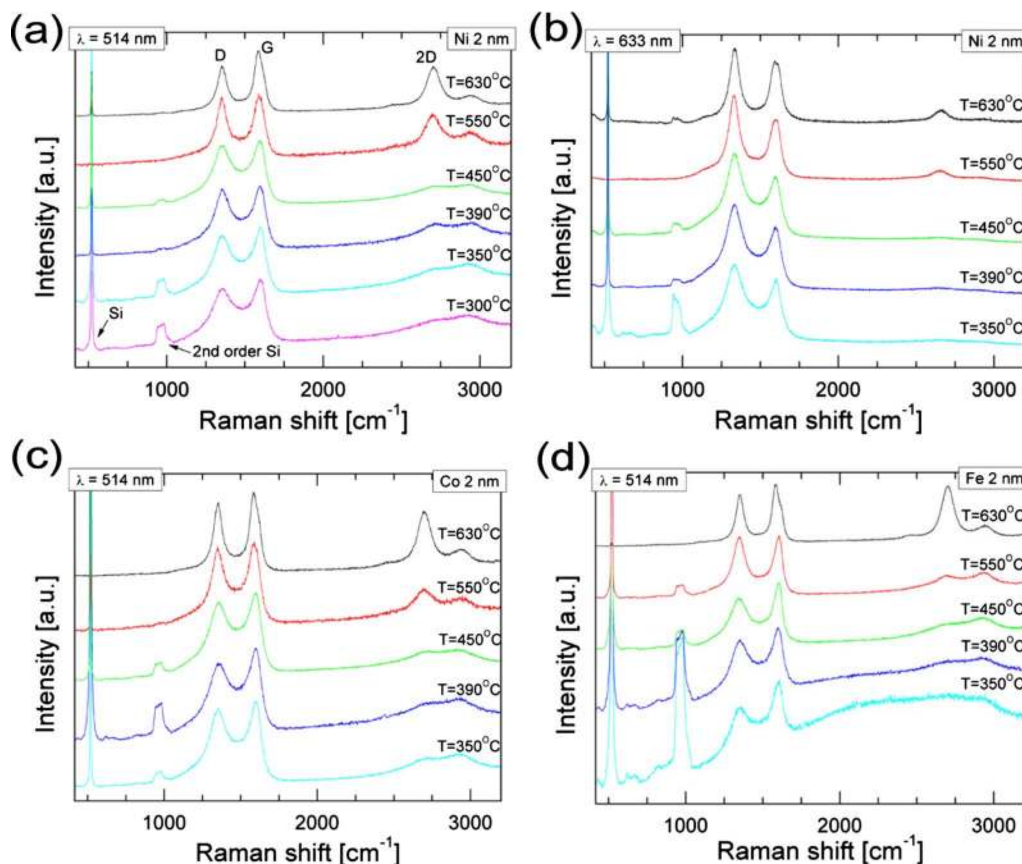

FIG. 12. (Color online) Raman spectra (514 and 633 nm laser excitations) of CNFs grown by thermal CVD from 2 nm [(a) and (b)] Ni, (c) Co, and (d) Fe films (NH_3 plasma pretreated). Relevant peaks are indexed.

Downloaded 24 Mar 2009 to 129.169.178.169. Redistribution subject to AIP license or copyright; see http://jap.aip.org/jap/copyright.jsp

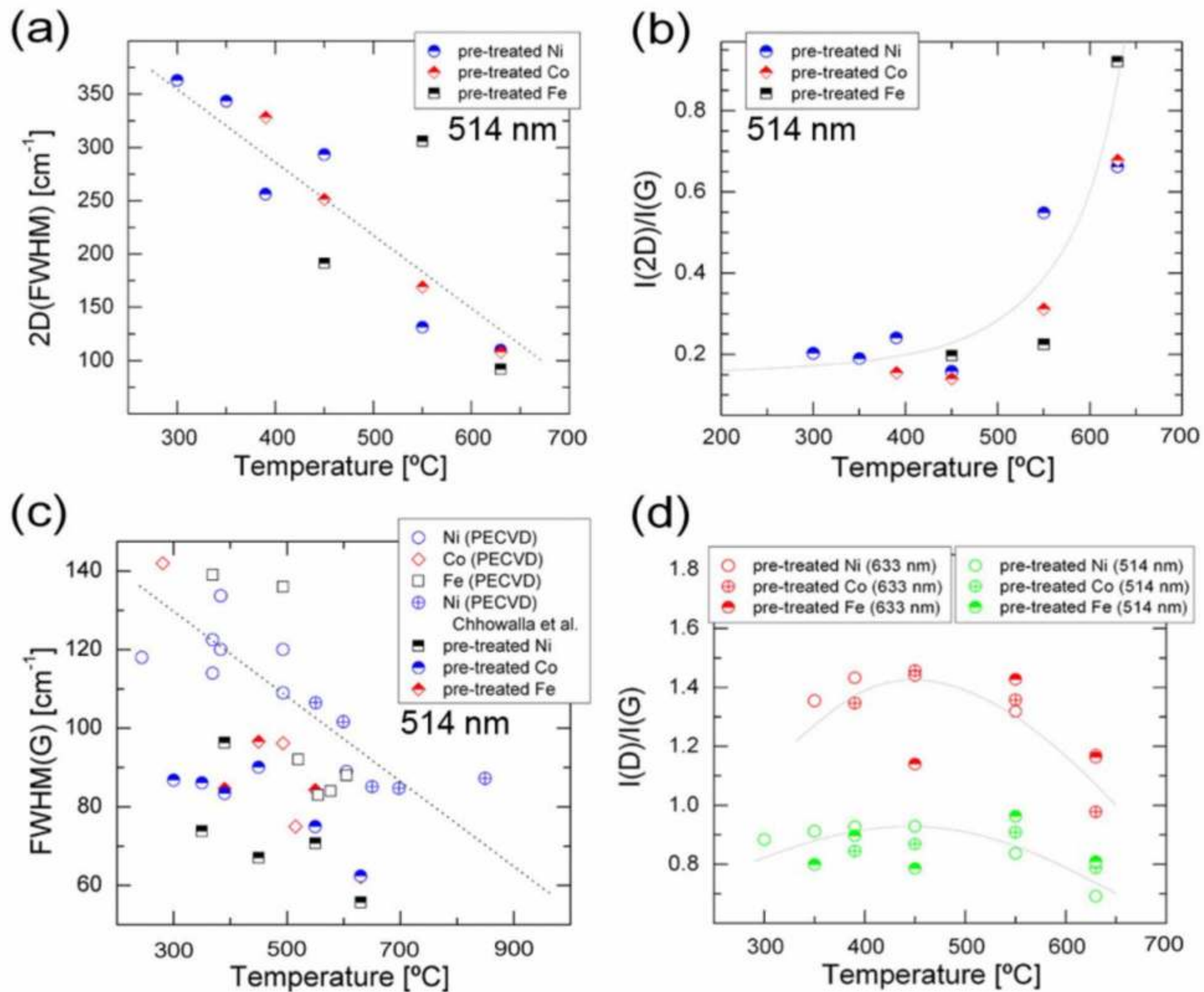

FIG. 13. (Color online) Raman analysis of CNF samples grown by thermal CVD from 2 nm Ni, Co, and Fe films. All plotted graphs refer to Raman spectra obtained with the 514.5 nm laser excitation, except for (f), where the 633 nm excitation is also considered. Lines are a guide for the eye only. Superimposed in (c)–(e) are the Raman data from nanotubes grown by dc-PECVD in same chamber from 6 nm Ni and 2 nm Co and Fe films (Ref. 25) and nanotubes grown by dc-PECVD from 6 nm Ni films by Chhowalla *et al.* (Ref. 22).

$I(D)/I(G)$ ratio was previously identified as a useful parameter to assess the crystalline quality of nanotubes.[22] We show here how for defective CNFs its dependence on temperature is not trivial and can be interpreted within the context of a more general framework. Additionally, other parameters [2D-peak full width at half maximum (FWHM), $I(2D)/I(G)$ ratio] are found to be relevant for the nanotube quality assessment.

We here compare our results to data obtained from samples grown by PECVD from Ni, Co, and Fe catalyst films in the low[48] and high temperature regimes, Figs. 13(c)–13(e).[22] The G and D peaks are fitted with Lorentzians. The 2D- and G-peak FWHMs increase as growth temperature decreases. The G-peak position decreases as growth temperature decreases [Fig. 13(c)].

If we isolate the contribution of thermally grown CNFs and evaluate the dependence of $I(D)/I(G)$ on the temperature for two different wavelengths (514.5 and 633 nm), a more clear trend emerges [Fig. 13(f)]. The behavior of the $I(D)/I(G)$ ratio versus temperature is not monotonic for both laser excitations used.

In carbon films the evolution from graphitic to nanocrystalline graphite ordering (e.g., for lower growth temperatures) is that the D peak and $I(D)/I(G)$ ratio increase, the latter following the Tuinstra–Koenig (TK) relation.[58] Also, the D' peak, at ~ 1620 cm^{-1} (shoulder of the G peak), appears but soon merges with the G peak as temperature lowers, so that both peaks can be fitted with a single Lorentzian, resulting in an effective blueshift in the G-peak position [Fig. 13(c)]. The size of the nanocrystalline domains, L_a, is inversely proportional to $I(D)/I(G)$ in this regime, but the TK equation experimentally holds for L_a down to ~ 2 nm.

Below 450–500 °C, defects are progressively induced in the nanotube structure. As defect density increases and L_a decreases, the number of ordered rings now decreases and $I(D)$ starts to decrease as well. The G peak relates only to bond stretching of sp^2 pairs, so its intensity remains constant, and the $I(D)/I(G)$ ratio decreases with increasing amorphization [Fig. 13(f)]. The increasingly amorphous character of the grown CNFs with decreasing temperature, as seen by HRTEM in Fig. 5, is now confirmed by Raman spectroscopy.

Downloaded 24 Mar 2009 to 129.169.178.169. Redistribution subject to AIP license or copyright; see http://jap.aip.org/jap/copyright.jsp

IV. CONCLUSIONS

In conclusion, we observed growth of CNFs at low temperatures by thermal CVD using thin Ni, Co, and Fe catalyst films. Films were subject to a NH_3 plasma pretreated for 5 min at ~600 °C (<15 W power) before CNF growth. A catalyst pretreatment is found to enhance the growth and density of CNFs, especially at low temperatures. We believe that this is due to the beneficial effect of the plasma on the restructuring of the catalyst film surface, activating more CNF nucleation sites with respect to films thermally annealed in NH_3 only. The crystallinity of the grown nanofibers reduces as growth temperature decreases, according to HRTEM and Raman spectroscopy.

ACKNOWLEDGMENTS

The work was supported by EU project CANAPE (Contract No. NMP-CT-2004-500096). S.H. acknowledges funding from Peterhouse, Cambridge, S.H. and A.C.F. from the Royal Society.

[1]B. Q. Wei, R. Vajtai, and P. M. Ajayan, Appl. Phys. Lett. **79**, 1172 (2001).
[2]M. Nihei, A. Kawabata, D. Kondo, and Y. Awano, Jpn. J. Appl. Phys., Part 1 **43**, 1856 (2004).
[3]F. Kreupl, A. P. Graham, M. Liebau, G. S. Duesberg, R. Seidel and E. Unger, Tech. Dig. - Int. Electron Devices Meet. **2004**, 683.
[4]R. H. Baughman, A. A. Zakhidov, and W. A. DeHeer, Science **297**, 787 (2002).
[5]J. Kong, H. T. Soh, A. M. Cassell, C. F. Quate, and H. J. Dai, Nature (London) **395**, 878 (1998).
[6]M. Endo, Y. A. Kim, T. Hayashi, K. Nishimura, T. Mtusita, K. Miyashita, and M. S. Dresselhaus, Carbon **39**, 1287 (2001).
[7]J. Koehne, J. Li, A. M. Cassell, H. Chen, Q. Ye, H. T. Ng, J. Haan, and M. Meyyappan, J. Mater. Chem. **14**, 676 (2004).
[8]W. I. Milne, K. B. K. Teo, G. A. J. Amaratunga, P. Legagneux, L. Gangloff, J. P. Schnell, V. Semet, V. T. Binh, and O. Gronning, J Mater. Chem **14**, 933 (2004); K. B. K. Teo, S. B. Lee, M. Chhowalla, V. Semet, V. T. Binh, O. Groning, M. Castignolles, A. Loiseau, G. Pirio, P. Legagneux, D. Pribat, D. G. Hasko, H. Ahmed, G. Amaratunga, and W. I. Milne, Nanotechnology **14**, 204 (2003).
[9]A. V. Melechko, V. I. Merkulov, T. E. McKnight, M. A. Guillorn, K. L. Klein, D. H. Lowdnes, and M. L. Simpson, J. Appl. Phys. **97**, 041301 (2005).
[10]W. R. Davis, R. J. Slawson, and G. B. Rigby, Nature (London) **171**, 756 (1953).
[11]R. T. K. Baker, J. Catal. **26**, 51 (1972).
[12]R. T. L. Baker, P. S. Harris, R. B. Thomas, and R. J. Waite, J. Catal. **30**, 86 (1973).
[13]R. T. L. Baker and M. A. Barber, *Chemistry and Physics of Carbon*, edited by P. L. Walker and P. A. Thrower (Dekker, New York, 1978), Vol. 14.
[14]M. S. Kim, N. M. Rodriguez, and R. T. K. Baker, J. Catal. **131**, 60 (1991).
[15]V. J. Kehrer and H. Leidhser, J. Phys. Chem. **58**, 550 (1954).
[16]L. M. J. E. Hofer, E. Stirling, and J. T. McCartney, J. Phys. Chem. **59**, 1153 (1955).
[17]P. A. Tesner, E. Y. Rabinovich, I. S. Rafalkes, and E. F. Arefieva, Carbon **8**, 435 (1970).
[18]R. T. K. Baker and R. J. Waite, J. Catal. **37**, 101 (1975).
[19]Z. F. Ren, Z. P. Huang, J. W. Xu, J. H. Wang, P. Bush, M. P. Siegal, and P. N. Provencio, Science **282**, 1105 (1998).
[20]V. I. Merkulov, D. H. Lowdnes, Y. Y. Wei, G. Eres, and E. Voekl, Appl. Phys. Lett. **76**, 3555 (2000).
[21]Z. P. Huang, J. W. Wu, Z. F. Ren, J. H. Wang, M. P. Siegel, and P. N. Provencio, Appl. Phys. Lett. **73**, 3845 (1998).
[22]M. Chhowalla, K. Teo, C. Ducati, N. L. Rupersinghe, G. Amaratunga, A. C. Ferrari, D. Roy, J. Robertson, and W. I. Milne, J. Appl. Phys. **90**, 5308 (2001).
[23]S. Hofmann, M. Cantoro, B. Kleinsorge, C. Casirasghi, A. Parvez, J. Robertson, and C. Ducati, J. Appl. Phys. **98**, 034308 (2005).
[24]S. Hofmann, R. Sharma, C. Ducati, G. Du, C. Mattevi, C. Cepek, M. Cantoro, S. Pisana, A. Parvez, F. Cervantes-Sodi, A. C. Ferrari, R. E. Dunin-Borkowski, S. Lizzi, L. Petaccia, A. Goldoni, and J. Robertson, Nano Lett. **7**, 602 (2007).
[25]S. Hofmann, C. Ducati, B. Kleinsorge, and J. Robertson, Appl. Phys. Lett. **83**, 135 (2003).
[26]M. Cantoro, S. Hofmann, S. Pisana, C. Ducati, A. Parvez, A. C. Ferrari, and J. Robertson, Diamond Relat. Mater. **15**, 1029 (2006).
[27]S. Hofmann, C. Ducati, B. Kleinsorge, and J. Robertson, Appl. Phys. Lett. **83**, 4661 (2003).
[28]M. Chen, C. M. Chen, S. C. Shi, and C. F. Chen, Jpn. J. Appl. Phys., Part 1 **42**, 614 (2003).
[29]T. M. Minea, S. Point, A. Granier, and M. Touzeau, Appl. Phys. Lett. **85**, 1244 (2004); S. Point and T. Minea, Diamond Relat. Mater. **14**, 891 (2005).
[30]K. Aoki, T. Yamamoto, H. Furata, T. Ikuno, S. Honda, M. Furuta, K. Oura, and T. Hirao, Jpn. J. Appl. Phys., Part 1 **45**, 5329 (2006).
[31]M. Cantoro, S. Hofmann, S. Pisana, V. Scardaci, A. Parvez, C. Ducati, A. C. Ferrari, A. M. Blackburn, K. Y. Wang, and J. Robertson, Nano Lett. **6**, 1107 (2006).
[32]S. Helveg, C. Lopez-Cartes, J. Sehested, P. L. Hansen, B. S. Clausen, J. R. Rostrup-Nielsen, F. Abild-Pedersen, and J. K. Norskov, Nature (London) **427**, 426 (2004).
[33]M. Lin, J. P. Y. Tan, and C. Boothroyd, Nano Lett. **7**, 2234 (2007).
[34]C. Mattevi, C. T. Wirth, S. Hofmann, R. Blume, M. Cantoro, C. Ducati, C. Cepek, M. Haevecker, A. Knop-Gericke, S. Milne, C. Castellarim-Cudia, A. Goldoni, R. Schlogl, and J. Robertson, J. Phys. Chem. C **112**, 12207 (2008).
[35]T. de los Arcos, M. G. Garnier, J. W. Seo, P. Oelhafen, V. Thommen, and D. Mathys, J. Phys. Chem. B **108**, 7728 (2004).
[36]S. Hofmann, R. Blume, C. T. Wirth, M. Cantoro, R. Sharma, C. Ducati, M. Haevecker, S. Zafeiratos, P. Schnerch, A. Osterreich, D. Teschner, M. Albrecht, A. Knop-Geriche, R. Schlogl, and J. Robertson, J. Phys. Chem. C **113**, 1648 (2009).
[37]A. C. Westerheim, A. C. Anderson, and M. J. Cima, Rev. Sci. Instrum. **63**, 2282 (1992).
[38]T. Mizutani, J. Vac. Sci. Technol. B **6**, 1671 (1988).
[39]C. V. Thompson, Annu. Rev. Mater. Sci. **30**, 159 (2000).
[40]S. Pisana, M. Cantoro, A. Parvez, S. Hofmann, A. C. Ferrari, and J. Robertson, Physica E (Amsterdam) **37**, 1 (2007).
[41]S. Hofmann, Nature Mater. **7**, 372 (2008).
[42]H. T. Cui, X. J. Yang, M. L. Simpson, D. H. Lowndes, and M. Varela, Appl. Phys. Lett. **84**, 4077 (2004).
[43]V. I. Merkulov, D. K. Henslye, A. V. Melechko, M. A. Guillom, D. H. Lowndes, and M. L. Simpson, J. Phys. Chem. B **106**, 10570 (2002).
[44]Y. Y. Wei, G. Eres, V. I. Merkulov, and D. H. Lowndes, Appl. Phys. Lett. **78**, 1394 (2001).
[45]K. B. K. Teo, M. Chhowalla, G. A. J. Amaratunga, W. I. Milne, D. G. Hasko, G. Pirio, P. Legagneux, F. Wyczisk, and D. Pribat, Appl. Phys. Lett. **79**, 1534 (2001).
[46]J. H. Choi, T. Y. Lee, S. H. Choi, J. H. Han, J. B. Yoo, C. Y. Park, T. Jung, S. G. Yu, W. Yi, I. T. Han, and J. M. Kim, Diamond Relat. Mater. **12**, 794 (2003).
[47]G. Y. Zhang, D. Mann, L. Zhang, A. Javey, Y. M. Li, E. Yenilmez, Q. Wang, J. P. McVittie, Y. Nishi, J. Gibbons, and H. J. Dai, Proc. Natl. Acad. Sci. U.S.A. **102**, 16141 (2005).
[48]M. Cantoro, S. Hofmann, S. Pisana, C. Ducati, A. Parvez, A. C. Ferrari, and J. Robertson, Diamond Relat. Mater. **15**, 1029 (2006).
[49]S. S. Fan, M. G. Chapline, N. R. Franklin, T. W. Tombler, A. M. Cassell, and H. J. Dai, Science **283**, 512 (1999).
[50]C. J. Lee and J. Park, Appl. Phys. Lett. **77**, 3397 (2000).
[51]C. Bower, O. Zhou, W. Zhu, D. J. Werder, and S. H. Lin, Appl. Phys. Lett. **77**, 2767 (2000).
[52]A. V. Melechko, V. I. Merkulov, D. H. Lowndes, M. A. Guillorn, and M. L. Simpson, Chem. Phys. Lett. **356**, 527 (2002).
[53]C. Ducati, I. Alexandrou, M. Chhowalla, J. Robertson, and G. A. J. Amaratunga, J. Appl. Phys. **95**, 6387 (2004).
[54]R. T. Yang and J. P. Chen, J. Catal. **115**, 52 (1989).
[55]R. T. Vang, K. Honkala, S. Dahl, E. K. Vestergaard, J. Schnadt, E. Laegsgaard, B. S. Clausen, J. K. Norskov, and F. Besenbacher, Nature Mater. **4**, 160 (2005).
[56]A. C. Ferrari and J. Robertson, Phys. Rev. B **61**, 14095 (2000).
[57]A. C. Ferrari and J. Robertson, Phys. Rev. B **64**, 075414 (2001).
[58]F. Tuinstra and J. L. Koenig, J. Chem. Phys. **53**, 1126 (1970).

Downloaded 24 Mar 2009 to 129.169.178.169. Redistribution subject to AIP license or copyright; see http://jap.aip.org/jap/copyright.jsp